

Investigation of the skin-friction drag reduction capabilities of wall-normal created plasma jets in wall-bounded turbulent flow

Atilla Altıntaş¹ ★ †, Lars Davidson¹ and Shia-Hui Peng¹⁻²

¹*Division of Fluid Dynamics, Department of Mechanics and Maritime Sciences*

Chalmers University of Technology, 412 96 Gothenburg, Sweden

²*Swedish Defence Research Agency, FOI, SE-164 90 Stockholm, Sweden*

*altintas@chalmers.se · lada@chalmers.se · peng@chalmers.se

†Corresponding author

Abstract

The plasma flow control is a promising technique for reducing aerodynamic drag on the surface of moving bodies, such as aircraft, resulting in improved fuel efficiency and speed. This study investigates the effectiveness of a wall-normal plasma jet in a turbulent channel flow by applying a force to the bottom wall of the channel. The goal is to suppress the formation or interaction of organized flow structures within the flow. The investigation is conducted for a frictional Reynolds number of $Re_\tau = 180$, and the skin friction drag reduction capabilities of the wall-normal plasma jet are analyzed for both applied force and no-force cases. The findings of this study suggest that wall-normal plasma jet flow has the potential to effectively reduce skin friction drag in turbulent flows. Despite the relatively low drag reduction achieved in this study (3%), further investigations are justified to optimize the parameters in order to achieve a larger drag reduction.

1. Introduction

Plasma jet flow is a technique used to reduce aerodynamic drag on the surface of a body moving through a fluid, such as an aircraft which results improvement on the fuel efficiency and speed of the vehicle. The technique involves the use of plasma discharge to generate a wall- aligned jet of fluid that interacts with the flow field and modifies it in a way that reduces the skin friction drag.¹

Recent studies have demonstrated the effectiveness of wall-aligned plasma jet flow in reducing drag in different flow scenarios, including turbulent boundary layers.² However, the potential of wall-normal plasma jet flow, created using plasma actuators, in terms of its drag reduction capabilities remains an area that requires investigation.³ The effectiveness of this technique depends on several factors, such as the size and shape of the plasma actuator, the applied voltage, the frequency of the discharge, and the properties of the fluid. The plasma actuator generates a plasma discharge that creates a jet of fluid that interacts with the flow field and modifies it in a way that reduces the skin friction drag.

In this study, we investigated the effectiveness of wall-normal applied plasma jet in a turbulent channel flow by applying a force to the bottom wall of the channel. Our goal was to suppress the formation or interaction of organized flow structures in the flow. This study was performed for a frictional Reynolds number of $Re_\tau = 180$. We examined the skin friction drag reduction capabilities of the wall-normal plasma jet by analyzing the applied force and no-force cases. To verify the results, we investigated changes in streak formations using tools such as velocity fluctuations and two-point correlations. Our findings suggest that wall-normal plasma jet flow has the potential to reduce skin friction drag in turbulent flow. The plasma actuator was found to suppress the formation and interaction of streamwise vortices, leading to a reduction on the drag. We hope that this study will contribute to the ongoing efforts to develop more efficient and effective methods for reducing aerodynamic drag.

2. Direct Numerical Simulations

A flow solver with an implicit, two-step time-advancement finite volume method is used.⁴ Central differencing is used in space and the Crank-Nicolson scheme is used in the time domain. When the Navier-Stokes the equation is

discretized for u_i it can be written as,

$$u_i^{n+1} = u_i^n + \Delta t H(u_i^n, u_i^{n+1}) - \frac{1}{\rho} \alpha \Delta t \frac{\partial p^{n+1}}{\partial x_i} - \frac{1}{\rho} (1 - \alpha) \Delta t \frac{\partial p^n}{\partial x_i} \quad (1)$$

where $H(u_i^n, u_i^{n+1})$ includes convection, the viscous and the source terms, and $\alpha = 0.5$ (Crank-Nicolson). Equation (1) is solved which gives u_i^{n+1} that does not satisfy continuity. An intermediate velocity field is computed by subtracting the implicit part of the pressure gradient, i.e.

$$u_i^* = u_i^{n+1} + \frac{1}{\rho} \alpha \Delta t \frac{\partial p^{n+1}}{\partial x_i}. \quad (2)$$

Taking the divergence of Eq. (2) requiring that continuity (for the face velocities which are obtained by linear interpolation) should be satisfied on level $n + 1$, i.e. $\partial u_{i,f}^{n+1} / \partial x_i = 0$, we obtain

$$\frac{\partial^2 p^{n+1}}{\partial x_i \partial x_i} = \frac{\rho}{\Delta t \alpha} \frac{\partial u_{i,f}^*}{\partial x_i}. \quad (3)$$

The numerical procedure at each time step can be summarized as follows.

1. Solve the discretized filtered Navier-Stokes equation for u , v and w .
2. Create an intermediate velocity field u_i^* from Eq. (2).
3. The Poisson equation (Eq. (3)) is solved with an efficient multigrid method `emvin:davidson:les`.
4. Compute the face velocities (which satisfy continuity) from the pressure and the intermediate velocity as

$$u_{i,f}^{n+1} = u_{i,f}^* - \frac{1}{\rho} \alpha \Delta t \left(\frac{\partial p^{n+1}}{\partial x_i} \right)_f. \quad (4)$$

5. Step (i) to (iv) is performed till convergence (normally two or three iterations) is reached. The convergence for the velocities is 10^{-7} and 10^{-5} for pressure. The residuals are computed using the $L1$ norm and they are scaled with the integrated streamwise volume flux (the continuity equation) and momentum flux (momentum equations).
6. Next time step.

DRAG REDUCTION BY PLASMA CREATED WALL-JETS

Note that although no explicit dissipation is added to prevent odd-even decoupling, an implicit dissipation is present. The intermediate velocity field is computed at the *cell centers* (see Eq. (2)) subtracting a pressure gradient. Then, after having solved the pressure Poisson equation, the face velocity field is computed, and the pressure gradient at the *faces* (see Eq. (4)) is added. This is very similar to the Rhie-Chow dissipation.⁵

3. Methodology

3.1 Shyy model for single DBD actuator

The Shyy model creates an electric field vector, \mathbf{E} , generated by a DBD plasma actuator, which is given as:

$$E(y, z) = E_0 - \frac{E_0 - E_b}{b} z^+ - \frac{E_0 - E_b}{b \tan(\theta)} y^+ \quad (5)$$

Equation (5) is divided into wall-normal and spanwise components, multiplied by a factor Dc

$$E_z(y, z) = DcE(y, z) \cos \theta, \quad (6)$$

$$E_y(y, z) = DcE(y, z) \sin \theta. \quad (7)$$

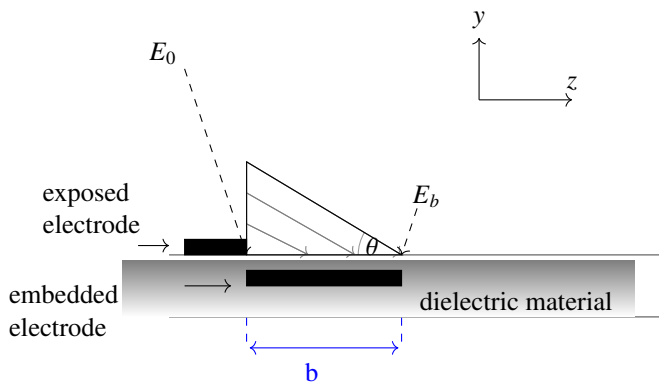


Figure 1: Shyy model illustration. Electric field strength, $E(y, z)$.

The parameter Dc is defined as the ratio of the electrical force to the inertial force, given by the equation $Dc = \frac{q_0 E_0 \delta}{\rho u \tau}$. Here, q_0 represents the maximum electron charge density. E_0 corresponds to the maximum electric field strength, which decreases along the embedded electrode until it reaches the breakdown strength E_b at the other edge (refer to

Figure 1). The quantities δ , ρ , and u_τ represent half the channel height, fluid density, and friction velocity, respectively.

In this study, the values chosen are $E_0 = 1.0$ and $E_b = 0.1$. The length of the plasma area is denoted by b , and the height of the plasma area is set as $b; \tan(\theta)$. In the study conducted by Shyy et al.,⁶ the plasma area was created in both the wall-normal (y) and streamwise (x) directions. However, in this study, the actuators are oriented in the spanwise direction, resulting in the force being generated in the y and z directions.

3.2 Validation of the Shyy model

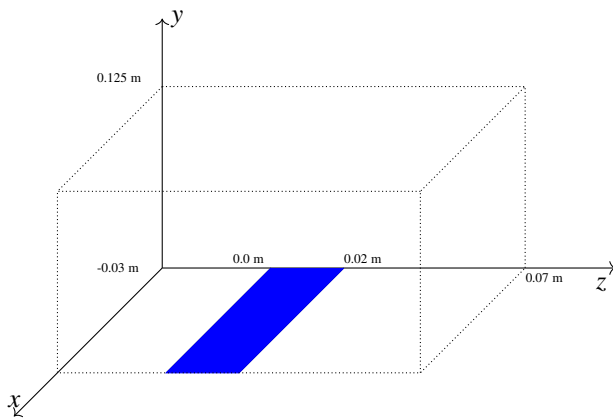


Figure 2: The location of the embedded electrode for the single DBD actuator.

The numerical model is compared to experimental data in a stationary flow with a single DBD actuator. Both experimental and computational fluid dynamics (CFD) results were obtained using a single DBD actuator. The experimental study, conducted by Benard et al.,⁷ applied a voltage of 12 kV and an AC frequency of 1000 Hz.

A two-dimensional study in a channel is performed, as shown in Fig 2. Equations 6 and 7 are solved in two dimensions (along the y and z directions), and the solution is iterated until a steady state is reached. Slip boundary conditions are applied in the actuator-aligned direction (z) and at the top boundary (high y). The fluid viscosity, $\nu = 1.81 \times 10^{-5}; m^2/s$, and density, $\rho = 1.25; kg/m^3$, are specified. Only the spanwise-directed component of the force is considered ($\theta = 0$), so only Equation 6 is applied, and $E_y = 0$ (i.e., Equation (2) is set to zero). This approach is similar to the model proposed by Greenblatt et al.,⁸ where a mean body force acts only in the plasma-aligned direction. The computational domain has dimensions of 125 mm \times 100 mm, as shown in Figure 1, with grid sizes of 98×298 ($y \times z$) for the wall-normal and plasma-aligned directions, respectively. The minimum and maximum grid sizes are $\Delta y_{min} = 0.00025$ m and $\Delta y_{max} = 0.0025$ m, with a stretching factor of $y = 1.35$ in the wall-normal direction. The

DRAG REDUCTION BY PLASMA CREATED WALL-JETS

grid size in the plasma-aligned direction is $\Delta z = 0.00033$ m. The oscillating force is applied in the plasma region ($0.0 < z < 0.02$ m, $0.0 < y < 0.0028$ m). The length of the plasma is $b = 20$ mm, and its location is illustrated in blue in Fig 2. The plasma region is discretized using 30×6 cells in the plasma-aligned and wall-normal directions, respectively.

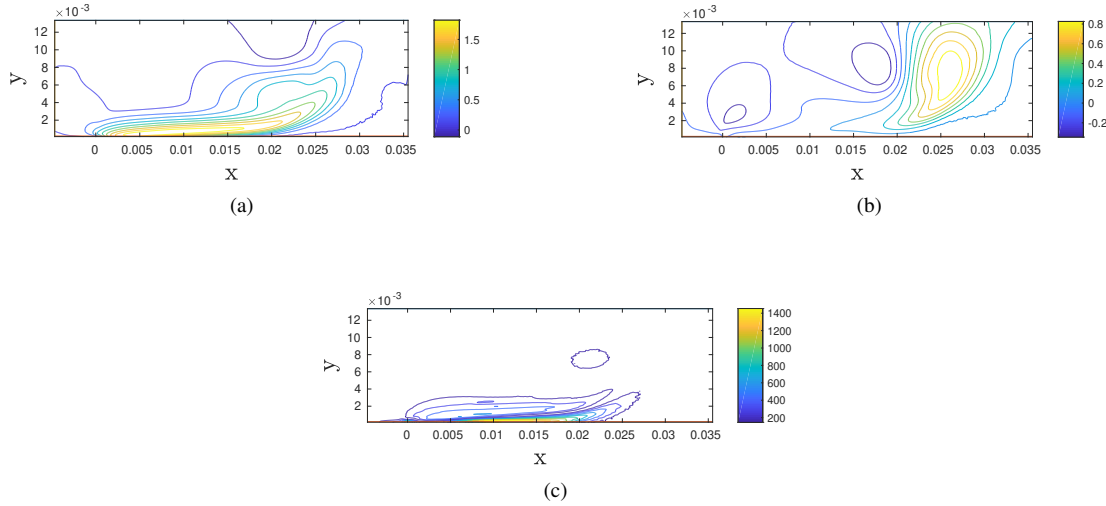


Figure 3: Experiments.⁷ (a) Plasma-aligned velocity, w . (b) wall-normal velocity, v . (c) vorticity.

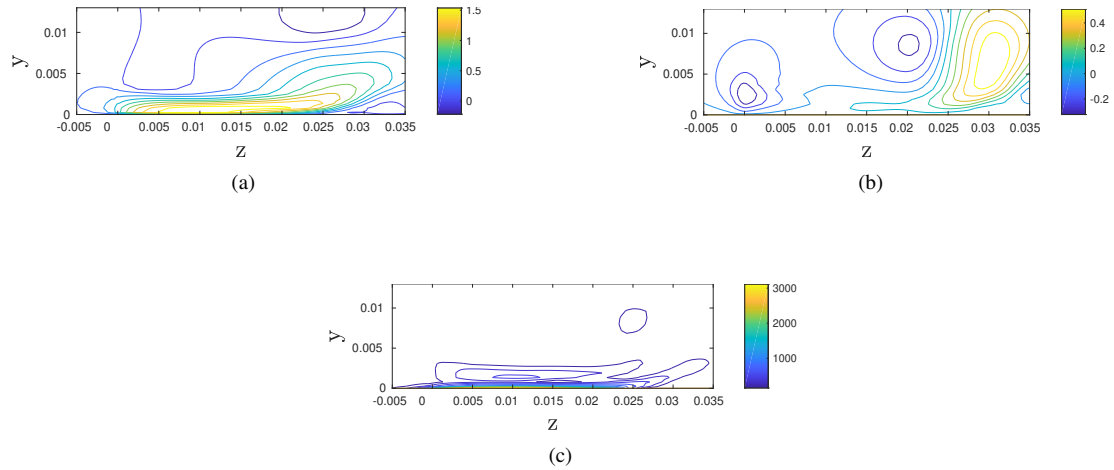


Figure 4: Numerical study. (a) Plasma-aligned velocity, w . (b) wall-normal velocity, v . (c) vorticity.

The predicted velocities of the ionized airflow exhibit a very similar behavior compared to the experimental data, as shown in Figures 3 and 4. The presence of the plasma region creates a negative wall-normal velocity upstream of the actuator and a positive wall-normal velocity downstream of the actuator (Figures 3(a) and 4(a)). The negative area entrains the flow towards the wall, while the positive area downstream of the actuator creates a wall jet that propagates downstream with a velocity parallel to the actuator (Figures 3(b) and 4(b)). Large vorticity is generated in the shear

layer above the actuator (Figures 3(c) and 4(c)). In the experimental study, the maximum plasma-aligned velocity is 1.8 m/s, and the wall-normal velocity is half that, at 0.9 m/s. The magnitude of vorticity is 1400. In the numerical study, we obtain similar velocity and vorticity fields compared to the experiments.

3.3 Wall-normal jet actuator design by opposing DBD actuators

The actuator that is used in this study is consist of two identical single DBD plasma actuators positioned opposite to each other with a gap area in between Fig. 5. The purpose of this arrangement is to generate a wall-normal jet flow in the middle of the actuator, when a high-voltage AC signal is applied to the actuators Figs. 6(a)-6(d).

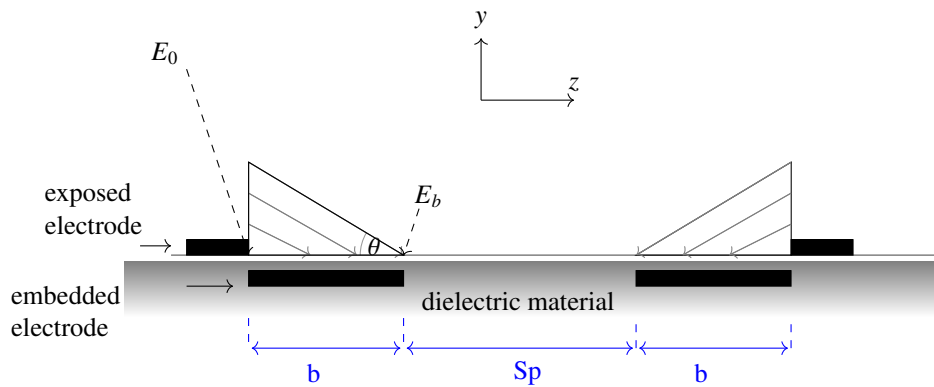


Figure 5: Illustration of opposed actuators to create a wall-normal jet.

DRAG REDUCTION BY PLASMA CREATED WALL-JETS

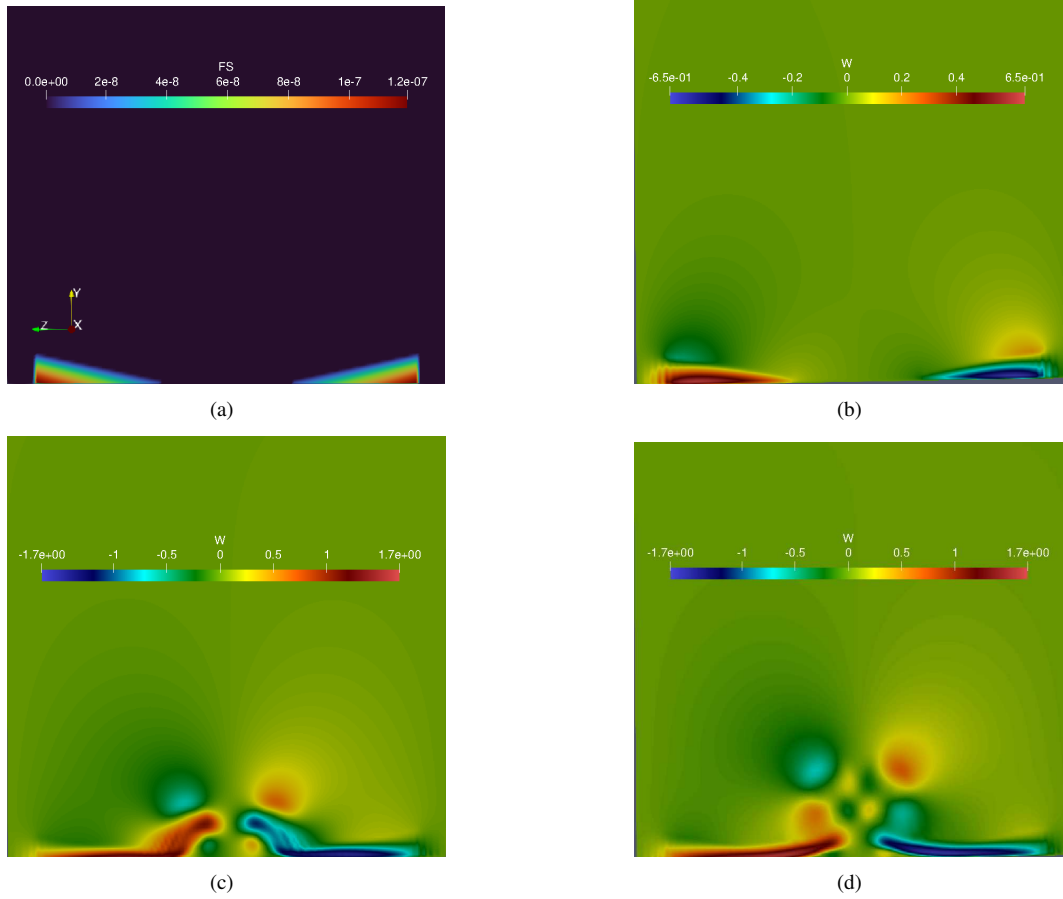


Figure 6: Created force and flow. (a) Force. (b)-(d) Plasma-aligned velocity evolution with time, which shows the creation of the wall-jet.

4. Multiple Actuator Configuration for DNS

4.1 DNS Settings

A DNS is performed to investigate the effects of multiple plasma actuators aligned in the spanwise direction. The aim is to generate a controlled body force to manipulate the flow.

A constant volumetric driving force is used in the streamwise momentum equation by which the frictional Reynolds number, $Re_\tau = 180$ is prescribed. Periodic boundary conditions are used in the streamwise and spanwise directions, while the usual no-slip boundary conditions are enforced at the walls. The domain size is $2\pi\delta \times 2\delta \times \pi\delta$ with grid size $98 \times 98 \times 194$ in the streamwise, wall-normal and spanwise directions, respectively. The grid resolution is $\Delta x^+ \approx 11.5$, $\Delta z^+ \approx 2.9$, and a stretching of 1.03 is used in the wall-normal direction. The nondimensional time step was kept smaller than $\Delta t^+ = \Delta t u_\tau^2 / \nu = 0.6$.

4.2 Multiple actuator design

The specific configuration of the actuators is shown in Fig 7. To simplify the analysis, only the spanwise component of the body force is considered, which means the force acts solely in the spanwise direction ($\theta = 0$ or $F_y = 0$). This simplification allows for a focused examination of the influence of the plasma actuators on the flow behavior.

The length of the plasma area, denoted as b , is chosen to be 5 computational cells. This corresponds to a dimensionless length of $b^+ = \frac{bu_\tau}{\nu} = 14.5$ for a given friction Reynolds number of $Re_\tau = 180$. This defines the maximum width of the plasma region in the spanwise direction for a single DBD actuator.

To space the plasma actuators appropriately, a spanwise spacing, S_p , is implemented in between opposed plasma areas, which is set equal to twice the length of the single plasma area (b^+). There are also a spacing between the 9 actuator pairs, which is equal to %20 of a single plasma area (b^+). The spacing, resulting in a total of 9 plasma actuators being employed in this study Fig.7(a). The specific arrangement and distribution of the actuators are determined based on this configuration. The creation of the force in the flow field is given in the Fig. 7(b).

For the simulations, a dimensionless parameter Dc is set to a value of 1.0, representing the ratio of the electrical force to the inertial force in the system. This choice of Dc influences the intensity of the generated body force and its impact on the flow.

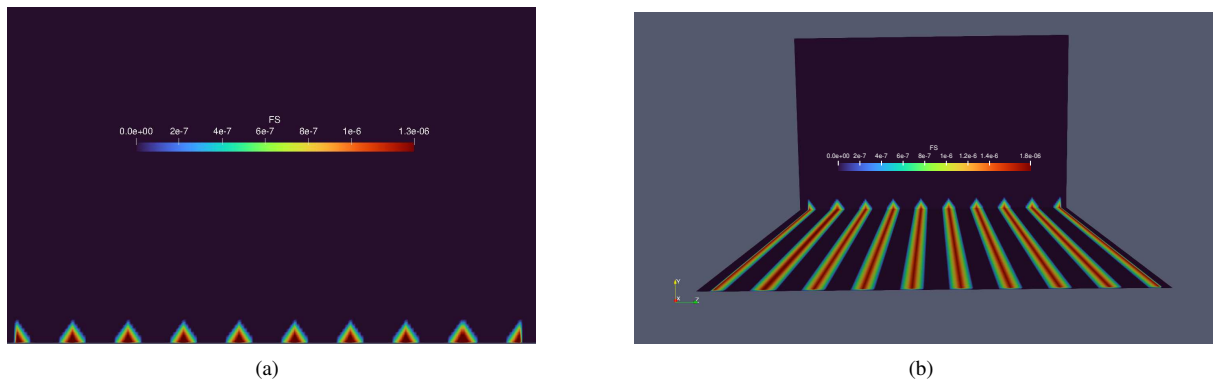


Figure 7: The plasma force is created in the south wall of the channel by using multiple actuators. (a) 9 actuator pairs are used. (b) Applied force.

5. Results

The analysis reveals that the implementation of the plasma actuators results in a modest reduction in drag, approximately 3%. Although the drag reduction achieved in this study is relatively low, it provides valuable insights into the

DRAG REDUCTION BY PLASMA CREATED WALL-JETS

potential effects and limitations of the employed plasma actuator configuration.

Figure 8(a) presents the mean velocity for the force and the no-force cases, compared with DNS data.⁹ We have not observed any change on the mean flow. A slightly lower streamwise velocity fluctuations, u_{rms} , and wall-normal velocity fluctuations, v_{rms} , are observed for the applied force case compared to the no-force case (Fig. 8(b) and 8(c)). For the applied force case, the spanwise velocity fluctuations, w_{rms} , are lower for the force applied case compared to no-force case Fig. 8(d)).

Figure 9, presents the Reynolds shear stresses for the force and no-force cases. A reduction approximately at $y^+ = 20$ till $y^+ = 90$ is observed, which results a reduction on drag.

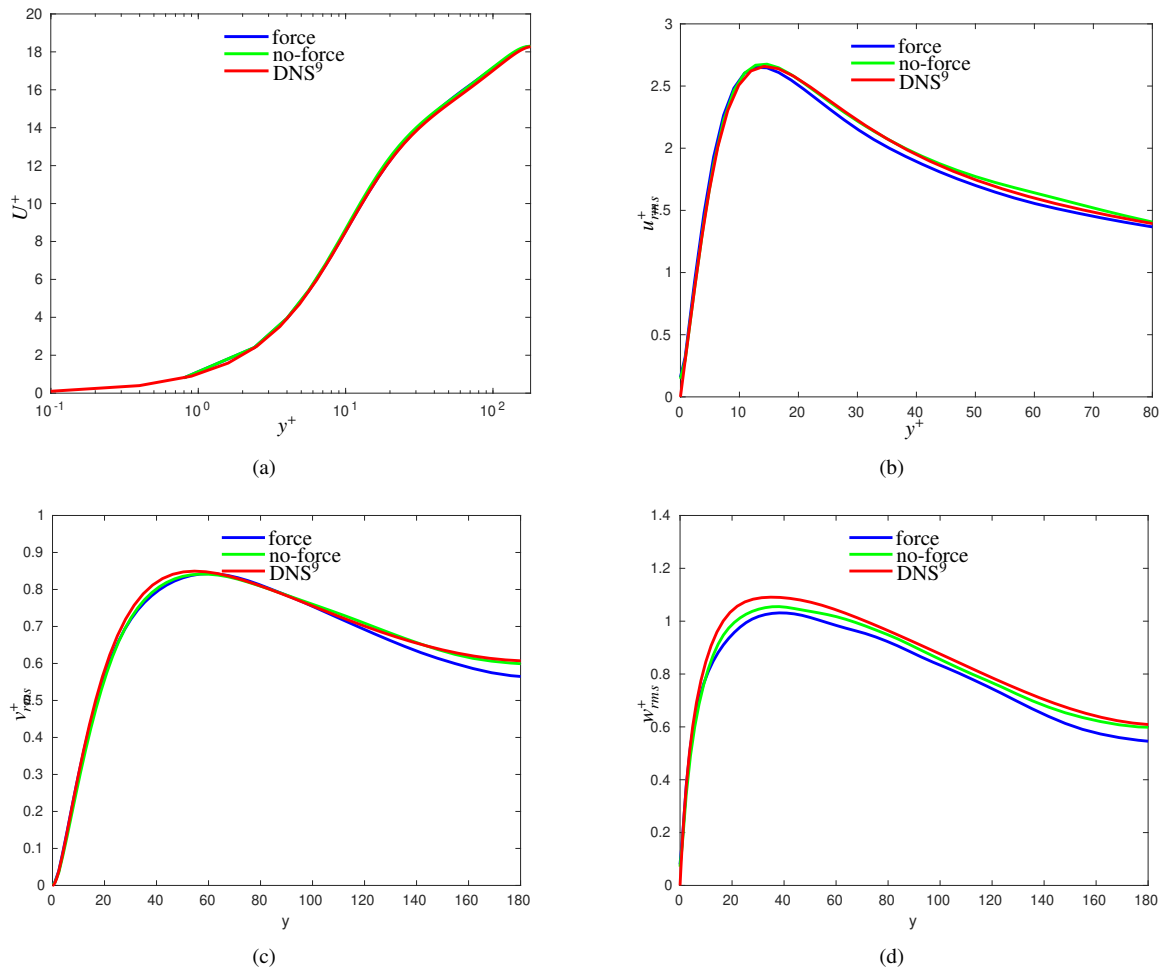


Figure 8: Mean and fluctuation velocities. (a) Mean velocity. (b) Streamwise velocity rms, u_{rms}^+ . (c) Wall-normal velocity rms, v_{rms}^+ . (d) Spanwise velocity rms, w_{rms}^+ .

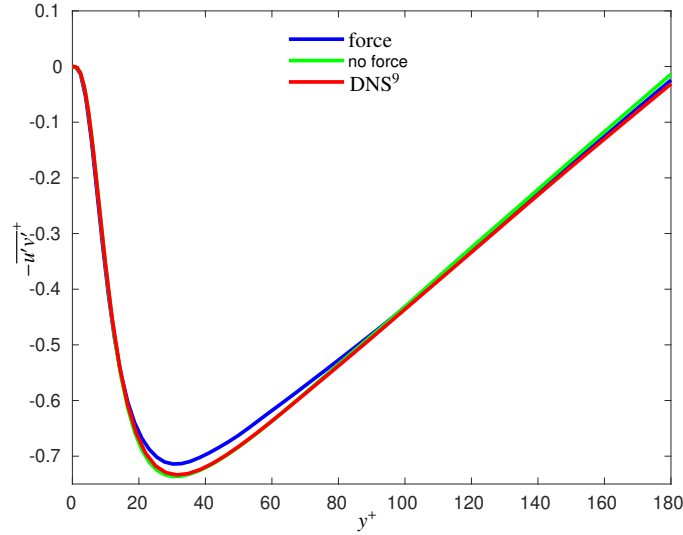


Figure 9: Reynolds shear stress.

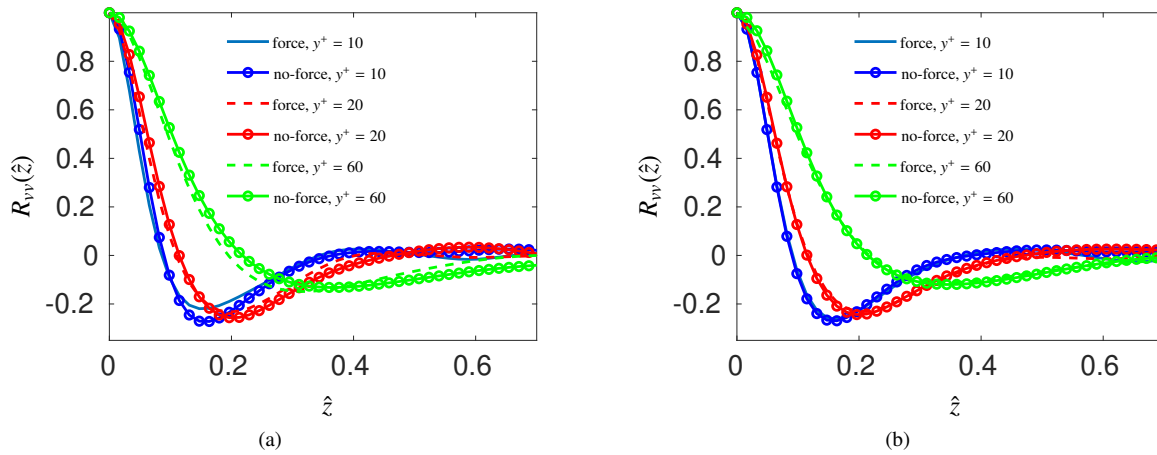


Figure 10: Wall-normal two-point velocity correlation for force applied case. (a) South wall. (b) North wall.

The presence of a minimum in the profiles of the wall-normal two-point velocity correlation in the spanwise direction, $R_{vv}(z)$, is indicative of the existence of streamwise vortical structures in the wall region.¹⁰ These structures can be characterized by a mean vortex structure, which is defined based on the time-averaged positions of the local minimum and maximum of the streamwise root mean square (rms) vorticity. The occurrence of the minimum in $R_{vv}(z)$ is directly related to the average spanwise distance across a vortex.

In Figure 10(a), where the values of $R_{vv}(z)$ are plotted for the south wall, it is observed that there is a decrease in the correlation for $y^+ = 10$, while preserving the same y^+ location, when compared to the no-force cases. This implies that the applied force influences the strength of the mean streamwise vortices near the wall, while the mean separation between vortices remains largely unaffected. In other words, the force alters the intensity of the vortical structures

DRAG REDUCTION BY PLASMA CREATED WALL-JETS

without significantly affecting their spatial arrangement.

Figure 10(b) illustrates the values of $R_{vv}(z)$ for the upper half of the channel. The values for the applied force cases closely align with the values obtained in the no-force cases.

6. Conclusions

In conclusion, this study investigated the effectiveness of a wall-normal plasma jet flow in reducing aerodynamic drag in turbulent channel flow. The analysis was conducted for a frictional Reynolds number of $Re_\tau = 180$, with a focus on suppressing the formation and interaction of organized flow structures within the flow.

The findings of this study indicate that the implementation of plasma actuators can lead to a modest reduction in drag, approximately 3%. Although the achieved drag reduction is relatively low, it provides valuable insights into the potential effects and limitations of the employed plasma actuator configuration.

The flow analysis revealed that slightly lower streamwise velocity fluctuations (u_{rms}) and wall-normal velocity fluctuations (v_{rms}) were observed in the force-applied case compared to the no-force case (Figure 8(b) and 8(c)). Additionally, spanwise velocity fluctuations (w_{rms}) were lower in the force-applied case compared to the no-force case (Figure 8(d)).

The actuator model and design of their multiple placement in a turbulent channel flow offers potential applications in various fields, such as aerodynamics, boundary layer control, and flow separation control. The controlled wall-normal jet flow can be utilized to reduce drag, or manipulate the flow characteristics for improved performance in specific applications.

Further investigations can be conducted to explore alternative configurations, optimize the parameters, and assess the performance of different plasma actuator arrangements for achieving more significant drag reduction and flow control in various practical applications.

References

- [1] A Altıntaş, L Davidson, and S-H Peng. Direct numerical simulation of drag reduction by spanwise oscillating dielectric barrier discharge plasma force. *Physics of Fluids*, 32(7), 2020.

- [2] Srikar Yadala, Marc T. Hehner, Jacopo Serpieri, Nicolas Benard, and Marios Kotsonis. Plasma-based forcing strategies for control of crossflow instabilities. *AIAA Journal*, 59(9):3406–3416, 2021.
- [3] X.Q. Cheng, C.W. Wong, F. Hussain, W. Schröder, and Y. Zhou. Flat plate drag reduction using plasma-generated streamwise vortices. *Journal of Fluid Mechanics*, 918:A24, 2021.
- [4] L. Davidson and S-H. Peng. Hybrid LES-RANS: A one-equation SGS model combined with a $k - w$ model for predicting recirculating flows. *Int. J. Numer. Fluids*, 43(9):1003–1018, 2003.
- [5] C. M. Rhie and W. L. Chow. Numerical study of the turbulent flow past an airfoil with trailing edge separation. *AIAA J.*, 2:1525–1532, 1983.
- [6] W Shyy, B Jayaraman, and A Andersson. Modeling of glow discharge-induced fluid dynamics. *Journal of applied physics*, 92(11):6434–6443, 2002.
- [7] N Benard, M Caron, and E Moreau. Evaluation of the time-resolved EHD force produced by a plasma actuator by particle image velocimetry-a parametric study. In *Journal of Physics: Conference Series*, volume 646, page 012055. IOP Publishing, 2015.
- [8] David Greenblatt, Torsten Schneider, and Chan Yong Schüle. Mechanism of flow separation control using plasma actuation. *Physics of Fluids*, 24(7):077102, 2012.
- [9] J. Jiménez and A. Pinelli. The autonomous cycle of near-wall turbulence. *J. Fluid Mech.*, 389:335–359, 1999.
- [10] J. Kim, P. Moin, and R. Moser. Turbulence statistics in fully developed channel flow at low Reynolds number. *J. Fluid Mech.*, 177:133–166, 1987.